International Journal of Hydrogen Energy 80 (2024) 1124–1136

Contents lists available at ScienceDirect

International Journal of Hydrogen Energy

journal homepage: www.elsevier.com/locate/he

# A comparison of multi-source power supply systems for autonomous marine vehicles: The SWAMP case study

A. Riccobono [c], V. Boscaino [a,*], A. Odetti [b], F.P. Mammana [c], G. Cipriani [c], G. Bruzzone [b], V. Di Dio [c], M. Caccia [b], G. Tinè [a]

[a] Institute of Marine Engineering, National Research Council of Italy, via Ugo La Malfa, 153, 90146, Palermo, Italy
[b] Institute of Marine Engineering, National Research Council of Italy, via De Marini 6, 16149, Genoa, Italy
[c] Department of Engineering, University of Palermo, viale delle scienze - edificio 9, 90128, Palermo, Italy

ARTICLE INFO

Handling Editor: Prof B Shabani

*Keywords:*
Autonomous surface marine vehicle
Lithium batteries
Fuel cell
Hydrogen energy
Photovoltaic source
Renewable energy

ABSTRACT

Extensive research on zero-emissions autonomous surface vehicles has been recently carried out, aiming at increasing autonomy. Due to their small size, unmanned vehicles present unique difficulties in terms of weight and dimensions when powering the vehicle with renewable energy sources. In this paper, photovoltaic source, fuel cell and Li-ion battery multi-source configurations are proposed, demonstrating by physical layout and simulation results the feasibility of the prototype, compliant with strict constraints of the vehicle under test. The energy system model of the vehicle under test is implemented in MATLAB/Simulink. A comparison of multi-source energy system configurations is proposed and validated by simulation results in terms of endurance, weight and size. If compared with the original battery-powered vehicle, as shown by comparing simulation results, the endurance is doubled, extended up to 12 h on the most favorable day of the year. The solution even complies with payload and physical dimensions constraints.

NOMENCLATURE

| | |
|---|---|
| SWAMP | Shallow Water Autonomous Multipurpose Platform |
| CHG | Greenhouse Gas |
| IMO | International Maritime Organization |
| RES | Renewable Energy Sources |
| ASV | Autonomous Surface Vehicles |
| PV | Photovoltaic |
| USV | Unmanned Surface Vehicle |
| DC | Direct Current |
| PVGIS | Photovoltaic Geographical Information System |
| SOC | State Of Charge |
| PM | Power Management |
| PFC | Fuel Cell power threshold |
| DoD | Depth of Discharge |

## 1. Introduction

International organizations and national governments have been compelled to adopt policies to reduce greenhouse gas (GHG) emissions, especially CO2, because of global warming. The proliferation of smart grid based on several Renewable Energy Sources (RES) is a feasible solution to increase the renewable generated power. Fuel cell, PV, wind and biomass are the most common sources in smart grids and electric vehicles parking lots [1,2]. These are consolidated applications where an electrolyzer could operate as a DC load and energy storage device or the fuel cell as a RES. The maritime sector is still an open research topic in terms of RES power supply. According to published reports and strategies from the International Maritime Organization (IMO), GHG emissions of total shipping grew nearly by 10% between 2012 and 2018 [3,4]. IMO relates the growing trend in CO2 emissions for the maritime industry to the extensive use of fossil fuels for shipping, aiming at reducing emissions by half by 2050 if compared to 2008 levels [4–6]. The adoption and responsible use of all renewable energy sources is widely promoted to achieve sustainable development. The modern IMO strategy recommends combining several solutions, primarily based on increasing the amount of power generated from Renewable Energy Sources (RES) [3,4]. In the last few years, research projects concerning autonomous surface vehicles (ASV) are gaining more attention, moving technology from a theoretical design concept to widespread use. ASV are frequently employed in hydrological monitoring, marine surveillance,

* Corresponding author. Institute of Marine Engineering, National Research Council of Italy, via Ugo La Malfa, 153, 90146, Palermo, Italy.
*E-mail address:* valeria.boscaino@cnr.it (V. Boscaino).

https://doi.org/10.1016/j.ijhydene.2024.07.206
Received 18 April 2024; Received in revised form 10 July 2024; Accepted 13 July 2024
Available online 19 July 2024

coast patrol and other military and civil applications. Thanks to their speed and dexterity, ASVs can easily navigate shallow waters and narrow routes, perhaps hard for conventional vessels. ASVs are frequently cheap and lightweight on purpose and significantly broaden the field of operations. Additionally, marine disasters may cause economic losses, environmental harm and human casualties and in this direction the deployment of ASVs seems to be an affordable way to increase maritime safety and reduce environmental impact [5]. Cutting-edge instrumentation for remote environmental monitoring and seabed mapping may be readily installed on board of the ASVs [6–8].

In this paper, different configurations of multi-source power supply systems on the lightweight autonomous surface marine vehicle, namely the SWAMP (Shallow Water Autonomous Multipurpose Platform) are designed and compared. The comparison and results are well-founded being the same the vehicle under study. The original version of the SWAMP [9] is powered by Li-ion batteries. Field data collected during the water-based trial missions of the battery-powered version are used to simulate the instantaneous electrical demand of the SWAMP model. The reference missions have been chosen to represent all the allowed driving conditions of the vehicle under test: remotely controlled, programmed trajectory, over-speed and two or four motors active at the same trajectory. The energy system is then updated by adding a hydrogen fed fuel cell and a photovoltaic source. All configurations are compliant with weight, size, and volume requirements of the SWAMP ASV. A flexible, modular model is implemented in MATLAB/Simulink allowing to enable/disable photovoltaic source, select a power sharing algorithm and even select full or partial activation of the auxiliary on - board devices. The energy management system demonstrates remarkable modularity, smoothly adjusting to variations in PV source availability. PV, being the bulkiest and most unpredictable among onboard sources, poses unique challenges. Consequently, post-processed simulation results are analyzed to compare fuel cell-battery hybrid and PV-fuel cell-battery configurations.

The novelty of the paper also lies in the specific application, sizing criteria, power management algorithms and modelling approach. The specific application of the ASV poses new challenges and strict constraints on weight and dimensions of the whole power supply system. To solve these issues a specific sizing criterion has been adopted, choosing the fuel cell maximum power according to the average load power consumption instead of the peak power, as usually done because of the source high energy density. Power management algorithms are formulated, based on deterministic strategies to accommodate for the sizing method, ensuring to complete the water-based mission in the worst-case of 6 h. Additionally, PV modules are introduced, still accommodating for strict application constraints. Power management algorithms are formulated, self-accommodating in case of disabled PV modules. The modelling approach in MATLAB/Simulink is conceived as a modular and flexible test platform to validate several power management algorithms and allowing the introduction of other renewable sources. Thanks to the proposed model, simulations are carried out as closely as possible to the effective supply system operating conditions, ensuring to enter the test phase when confident with successful behavior under normal or unexpected conditions. In a bottom-up design flow, novelty starts from the application and extends to each step of the design and modelling approach. The proposed model includes primary sources, power converters and on-board electrical load. To solve time resolution discrepancies between the execution time of the reference missions (hours) and timing of converters operation (switching frequencies typically of hundreds of kHz), power converters are conveniently modelled by their typical conversion efficiency in order to simulate the overall reference mission.

In Section 2, an overview of the state of the art, including the most competitive marine surface vehicles is discussed. In Section 3, mechanical and energy system design of the ASV under study is described, focusing on the power architecture and the on-board sources size and ratings as well. The hybrid power supply model is described in Section 4. Simulation results are presented in Section 5. The comparison of multi-source configurations is discussed in Section 6 and conclusion are drawn in Section 7.

## 2. Overview of competitive marine vehicles

The use of fuel cell seems to be a feasible solution to meet decarbonization targets of the maritime industry and IMO long-term goals, because of their high energy density, fast refueling capability and zero emissions [10–16].

The cost of the fuel cell stack is still high, but the energy density is higher and higher than batteries. Recharging operation is extremely fast for fuel cell, consisting of replenishing the hydrogen tank. Batteries feature higher weight and lower energy density, and this limit their use. Proton Exchange Membrane Fuel Cells (PEMFC) are the most common in low-medium power applications. Pure hydrogen-fed fuel cells guarantee zero-emission, complying with the new regulations [3,4]. Fuel cell still exhibits higher and higher energy density if compared to battery, thus ensuring an enhancement of vehicle endurance. However, because fuel cells are sluggish to start and operate, using batteries as auxiliary sources is essential to ensure both high energy and power density [17–20]. Because of conflicting features of the fuel cell low power density and fast dynamic load transients in such an application, coupling with batteries is strongly recommended. A power management system is required to implement power sharing algorithms between sources to meet load power demand while preserving the state of health of both sources. In the literature, hybrid configurations and techniques, coupling the fuel cell with energy storage devices, are investigated for a wide variety of applications. Hybridization is required because of the slow transient response of the fuel cell stack, sensitivity to load variations and issues concerning cold start [19,21,22]. In the literature, hybrid configurations are commonly divided into active (coupled through DC-DC converters) and passive (directly connected) coupling between sources. In Ref. [23], a passive hybrid source for electric powertrains is proposed as the cheapest solution for hybridization. The fuel cell and the battery are directly connected to the bus. Voltage matching between sources is required. The source currents are self-regulated by their output impedance. The control of the fuel cell power is exploited by controlling its operating pressure, so varying its internal impedance, being constant the voltage operating value.

The active hybrid configuration consists of coupling the primary sources through active power converters. With the active power plant, power distribution and voltage alignment among sources can be actively managed. Peak power demands are managed by the battery, while the load on the fuel cell remains constant. The fuel cell converter is required to interface with the high voltage DC bus, as a high step-up DC/DC converter minimizing current ripple. A novel zero voltage switching high step-up multiphase interleaved boost converter is proposed in Ref. [24]. Low input current ripples, high voltage step-up ratio, soft-switching operation, and low switching harmonics and noise are achieved by the novel architecture [24].

Among active configurations, cascaded (semi-active) and DC common bus architecture could be implemented for low power applications. Semi-active configurations are implemented in Refs. [19,25]. In the semi-active configuration, a battery power converter is not required, and the battery is directly connected to the bus. Moreover, voltage matching between the fuel cell converter and the battery voltage should be achieved. Power sharing is achieved without the need for external components or algorithm implementation. Nonetheless, the architecture is scarcely modular in nature.

In this paper, active configuration is designed and implemented taking advantages from modularity and flexibility of the DC common bus architecture.

Power sharing methods based on deterministic rules are often referred to as rule-based algorithms. Rule-based algorithms usually act on a specific operation of the load power, equivalent hydrogen

consumption or also on the state of charge (SOC) of the battery system. Optimization-based sizing and power management algorithm are based on the optimization of a cost function, usually concerning system efficiency and/or fuel consumption [26–29]. Heuristic and optimization strategies are often based on the efficiency curve of the fuel cell stack and formulated to reduce hydrogen consumption enhancing the power sharing performances [29,30]. Several searching strategies like maximum power point tracking (MPPT) are proposed to face with fuel cell aging. In case of aging, the real-time algorithm is not affected by aging deviations, continuously seeking the most efficient operating point. However, optimization-based algorithms significantly increase controller complexity. This paper implements and compares low-complexity, rule-based algorithms. For future developments, optimization based algorithms are under consideration even to compare results in terms of endurance, hydrogen consumption and residual battery state of charge with rule-based algorithm.

In [31], an overview of hydrogen fed marine vehicles is given. Hydrogen production and storage techniques are discussed, including electrolyses from sea water. Safe issues are here solved by metal hydride canister. In Ref. [32], in order to favour endothermic hydrogen desorption, a thermal coupling system has been developed, in which a portion of the heat generated by the FC is transmitted to the metal hydride tank. Heat exchange is mandatory if high volumes of hydrogen are considered.

In [14], a weight-optimized hybrid fuel cell - battery system for a Swedish rescue boat is proposed. A detailed comparison of weight and volume for the hybrid system (75 kW PEM, 60 kWh battery pack) considering several systems with hydrogen fed source and battery is carried out. According to presented results, the hybrid system is significantly lighter than that of a battery system for all the hydrogen storage alternatives.

High endurance and low energy consumption are critical requirements. ASV are mainly operated by battery power, housing as many batteries as possible to extend the cruising range [33–35]. Undoubtedly, ASV establishes low weight and size limits on the entire power supply system. Extending cruising range by increasing the installed battery capacity results in bulky and inefficient marine vehicles, further reducing the available payload for on-board instrumentation. In Ref. [9], a survey of existing battery powered multihull ASV/USV is also addressed. According to the reported overview, the highest recorded endurance is obtained by the *CatOne*, which was updated to the *CatOne HD4* version, which measures 1.95 m × 1.34 m, features an empty weight of 30 kg, and up to 50 kg payload and ensures up to 8 h endurance, without specifying the capacity of installed batteries [36]. This is closely followed by the *OpenSwap*, that is equipped with four LiPOs battery pack of 20 Ah, ensuring up to 7 h endurance, as stated by authors [33]. As reported in Refs. [9,37] the battery-powered variant operates with two 13 Ah Li-ion rechargeable batteries at once, one for each hull, housed in a waterproof canister, with total dimensions of 1230 mm, nominal width of 1100 mm, and weight of 38 kg. Four battery packs are really installed but only two at once are used. Each watertight battery pack, weighing 3.4 kg, includes a 13 Ah battery pack in a 10S5P cell configuration. Hot-swapping battery packs allow adequate mission endurance. Due to the increased resistance coefficients in shallow water, slower speeds are required to keep constant the foreseen endurance or a shorter mission should be accounted for. If the SWAMP needs more power due to increased power consumption, longer trips, or extra payloads that demand a great deal of on-board power, additional power batteries may be easily mounted on the SWAMP. In Ref. [37], the extreme condition of operation at maximum auxiliary on – board subsystem is considered to evaluate benefits of introducing a hydrogen fuel cell in the on-board power system.

For effective on-board power generation and distribution, the pairing of fuel cells and batteries has been the focus of extensive studies [10,13,38–46]. Fuel cell technology still features lengthy start-up and slow dynamic response to load transients. Fast-changing dynamic loads can be accomplished by using batteries as storage energy sources with high power density.

In [39], an unmanned catamaran powered by hydrogen fuel cell is proposed and the design of a fuel cell - battery powered marine surface vehicle, by using a 200 W fuel cell stack equipped with a metal-hydride canister MH-350 by Horizon fuel cell, is clearly described not focusing on the endurance of the marine vehicle. As stated by authors, in marine surface vehicles, fuel cell systems are prone to higher dynamic load transients than those in aerial and submerged vehicles. These transients may deteriorate or even damage fuel cell sources owing to local gas starvation and flooding events. According to the installed energy systems, the fuel cell can directly charge the battery or contribute to the propulsion section load by means of properly installed relays, according to which maneuver is carried out [39].

Batteries help in handling the peak and transient power. Batteries can also aid in lowering the amount of consumed hydrogen. Even if batteries provide a zero-emission option, effective usage on lightweight vessels is severely constrained by their higher weight and poorer energy density. If hydrogen is produced from renewable energies, fuel cells benefit from lower environmental impact. As for batteries, fuel cells benefit from zero-emissions, low noise, and vibration, thus not affecting environmental ocean monitoring and the marine ecosystem. Fuel cells take advantages of higher energy density over batteries ensuring higher endurance values at the maximum on-board power and vehicle speed not affecting the system weight heavily.

In [37], an energy consumption modelling approach is adopted to accurately size on-board renewable sources and test power management algorithms. In Ref. [37], the minimum weight and cost solution, as determined by the optimization results, consists of a fuel cell with rated power roughly equal to the maximum value of the mean power consumption of the electrical load, averaged over the set of available recorded missions, and the smallest battery pack that can handle the extra-power requirement. Safety concerns are solved by metal hydride storage. Four power management algorithms are compared in terms of fuel cell performances and vehicle endurance by means of power consumption models. With almost the same on-board weight, endurance is extended to 6 h at maximum auxiliary load consumption, not requiring hot swapping of primary sources.

In [47], a state machine control for power management is described. In Ref. [47], preliminary results of system modelling in MATLAB environment are presented, but accounting for propulsion power consumption only.

## 3. The SWAMP case study

The SWAMP is a lightweight autonomous surface marine vehicle studied for operation in extremely shallow waters, featuring modularity and portability. The development of the SWAMP ASV stems from a collaborative effort between CNR-INM and DITEN-UNIGE [9]. In this paper, the mechanical and energy characteristics of the vehicle are assumed as a case study in sight of future developments and sea tests.

### 3.1. Mechanical construction of the SWAMP

The SWAMP is a novel autonomous surface vehicle (ASV) designed and developed for deployment in remote and extremely shallow aquatic environments. This highly adaptable and reconfigurable small and lightweight ASV possesses the capability to execute diverse tasks, including environmental monitoring, water sampling, bathymetric analysis, and water quality assessment.

Distinguished by its innovative use of soft materials to safeguard the propulsion system, electronics, and sensors, the SWAMP ASV incorporates a pump jet propulsion module housed within its hull and flush with it. Additionally, a multi-agent distributed guidance, navigation, and control system, enabling autonomous operation or collaborative missions with other vehicles is designed and implemented. SWAMP

hydrodynamic behavior has been highly studied as reported in Refs. [9, 48] with groundbreaking aspect of conducting comprehensive tests on an ASV within a towing tank, encompassing both shallow waters and self-propulsion. This breakthrough contributes significantly to enhancing our understanding of the ASV's hydrodynamic properties, which, in turn, facilitates the development of more effective control strategies. The studies enabled the determination of SWAMP hull's advance speed in both shallow and deep waters. Furthermore, the self-propulsion tests provided insights into the performance of the Pump-Jet Module under various advanced and rotational speeds. The test results underscored the need to strike a balance when designing a vehicle suitable for shallow water environments. This vehicle should offer a combination of features, including high payload capacity, low draft, easy transportability (lightweight and compact dimensions), extended endurance, and excellent modularity for various mission profiles. Achieving these objectives requires navigating the challenge of reconciling conflicting requirements. The design output, namely the perfect balance between these requirements, does not lead to the optimized solution but to optimum reachable. For this reason, further studies on the hull shape optimization have been performed by means of multi-fidelity hydrodynamic analysis at surveying speed in deep water subject to variable payload as reported in Ref. [49]. This study allowed to design a new hull and to calibrate the vehicle to minimize the resistance around the best operating conditions for different surveys. Fig. 1shows the vehicle SWAMP in its battery-operated version.

### 3.2. Energy system of the SWAMP

Strict limitations on the weight and size of the entire power supply system are imposed by the ASV application. A distinctive size criterion has been used to address these problems, sizing the fuel cell maximum power based on the average power consumption of the load rather than the peak power. Consequently, the fuel cell is not the highest priority source. Even introducing PV modules, a feasibility analysis from a physical and mechanical point of view is conducted, validating the multi-source architecture layout on-board of the SWAMP deck. In Ref. [37], the on-board power equipment has been accurately sized based on the proposed energy consumption model. As a result of the modelling and simulation results, the energy system consists of a fuel cell with rated power slightly higher than the maximum value of the mean power consumption of the electrical load, averaged over the set of available recorded missions. The hybrid system is designed by actively coupling the fuel cell with the smallest battery pack that can handle the extra-power. Front-end DC-DC converters in a common DC bus architecture are included. Safety concerns are solved by metal hydride storage.

The fuel cell - battery energy system consists of a 300 [W] fuel cell with a metal hydride cartridge as hydrogen reserve and a 36 [V]/15 [Ah] Li-ion battery. Two custom PV modules (72 Wp and 104 Wp), are included in the PV – Fuel cell – battery configuration. In Fig. 2 the physical layout shows all sources and hydrogen reserve on the SWAMP deck, measuring 1230 mm × 1100 mm. Dimensions are superimposed to highlight that each source fits the strict constraint on size. Marine grade flexible walk-on modules are selected according to the available size and payload of the SWAMP vehicle. By adding an extra-source, solar power contributes to SWAMP propulsion and auxiliary power demand. The on-board battery may be charged during missions, according to energy availability and instantaneous power demand, also by the PV modules, thus contributing to save the hydrogen reserve and extending the endurance of the vehicle. The highest priority level among available on-board sources is given to the solar power source, according to environmental operating conditions and instantaneous power demand. As shown in Fig. 2, the custom PV modules comply with size and volume constraints. Additionally, PV modules are introduced while adhering to stringent application requirements. As demonstrated in Fig. 2, the whole multi-source power supply system complies with strict constraints in terms of dimensions, fitting the available dimension of the SWAMP deck.

**Fig. 1.** The battery powered SWAMP vehicle.

Electrical characteristics and ratings, weight and dimensions specifications of the main components of the power equipment are listed in Table 1.

By using PVGIS online tool, irradiance and temperature dataset corresponding to a specific date and site (where water-based mission has been executed) are downloaded and used as input data of the model. The user can select a mission, a date and timestamp to start climate data import as the energy system model input. Irradiance and temperature data are extrapolated for four relevant dates: March 21, June 21, September 21 and December 21, 2019. The PV power production is then modelled by sing real PVGIS dataset.

The SWAMP vehicle is modelled by the overall instantaneous power consumption, which has been recorded during water-based missions of the battery-powered counterpart, including both the propulsion and the auxiliary parts. Fig. 3 shows the mission profiles recorded during four relevant water missions. Most relevant parameters of the four reference missions, namely SWAMP_A, SWAMP_B, SWAMP_C and SWAMP_D are listed in Table 2. SWAMP_A mission has been recorded in Camogli (Italy) on September 15, 2019, SWAMP_B and SWAMP_C in Biograd Na Moru (Croatia) on September 4 to October 4, 2019, respectively, and SWAMP_D mission in Roja (Italy) on November 5, 2019. All on-board auxiliary parts have been activated. The remotely controlled trajectory has been experienced with missions SWAMP_A and SWAMP_D, whereas the autonomous programmed trajectory has been experienced in missions SWAMP_B and SWAMP_C. SWAMP_A is critical because it lasts about 6 h, followed by mission SWAMP_B lasting about 5 h. During SWAMP_C the velocity of the vehicle overcomes 1.5 m/s, thus leading to an increase of the instantaneous peak power. Notwithstanding this, the mission is the shortest. SWAMP_D operates with all four motors on, thus leading to the highest peak power consumption. The four reference missions are representative of all allowed driving operating conditions: remotely controlled (SWAMP_A, SWAMP_D), trajectory programming (SWAMP B, SWAMP_C), over-speed (1.5 m/s) (SWAMP_C) and two (SWAMP_A,SWAMP_B) or four (SWAMP_C, SWAMP_D) motors active. All relevant driving conditions are represented by the four reference missions.

The energy section is designed by using a common DC bus architecture for enhanced flexibility and modularity. Each source is connected to the common DC bus through a front-end dedicated converter, providing for the source control and power sharing. The architecture features a high degree of modularity to allow expansion of the renewable energy quota.

Fig. 4 shows a block diagram of the designed energy section. A common DC bus architecture, featuring the highest flexibility and modularity if compared to cascaded or multiport connection is adopted. The system is modular even thanks to the definition of proper power management algorithm. A power management unit regulates the load power sharing, according to peculiar characteristics of each. The fuel cell source, which provides the highest energy density, ensures long endurance based on the on-board hydrogen reserve and load power

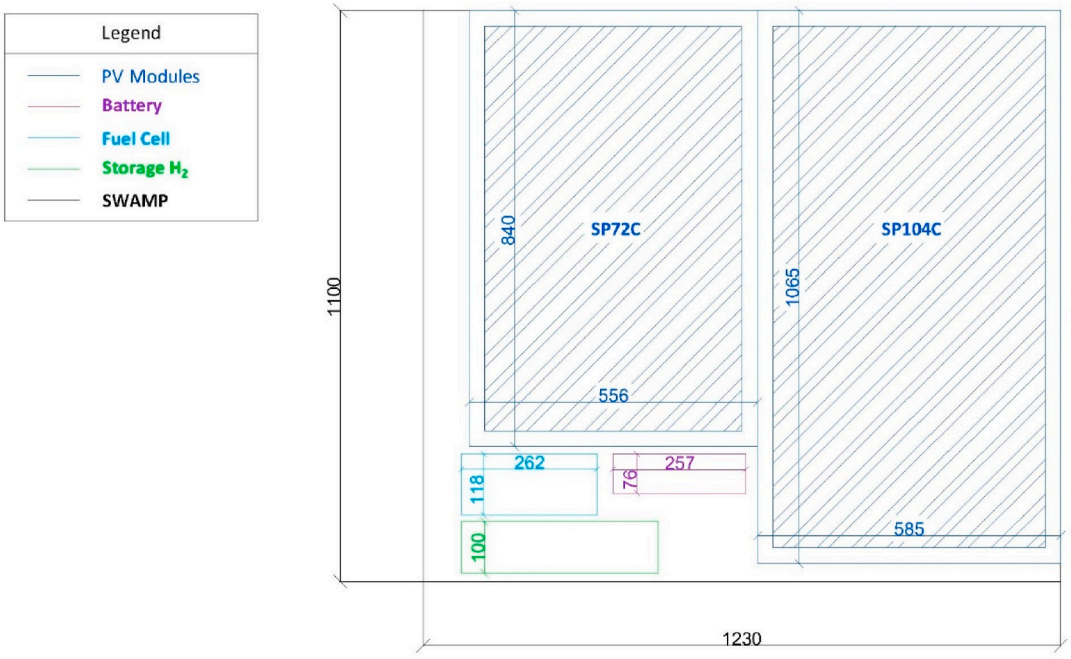


**Fig. 2.** Physical layout of multi-source energy system of the SWAMP vehicle.

demand. Applying load leveling to avoid fast load transients will boost endurance while ensuring the fuel cell safe operation. In accordance with the overall instantaneous power requirement of the vehicle, the battery will then source or sink the extra power quota. Based on field data such as the battery state of charge (SOC%), the instantaneous power produced by PV and the instantaneous load consumption ($P_{mission}$), the power management unit computes and transmits the active power thresholds of the battery $P_{battery}$ and fuel cell $P_{fc}$. The power management unit can also disable the PV source, according to the power sharing algorithm and sources priorities. Each front-end converter sets the source equivalent load by properly controlling the source current limit after receiving the active power threshold information. By removing the solar modules, the algorithm is automatically adapted to the new configuration without modifying the algorithm code. The power management unit fixes the power setpoint of each source according to the implemented power sharing algorithm. The user can select to activate auxiliary parts, even partially compared to total on board devices. The selected active parts power consumption is included in the overall mission power profile. The selection of activated auxiliary parts, at the simulation stage, is demanded to the user. However, in the near future, during sea trials, this information could be automatically transmitted by the SWAMP vehicle to the land station.

To account for the sizing approach, power management algorithms are developed based on deterministic strategies, guaranteeing that the water-based mission will be completed in the worst-case scenario of 6 h with fuel cell – battery configuration and up to 12 h endurance if PV modules are enabled. This paper focuses on two rule-based power sharing algorithms. The proposed algorithms will be compared in terms of both endurance and safety of fuel cell operations. The first algorithm, namely PM1 gives priority to the solar power than to the fuel cell and finally the battery source.

If the instantaneous power demand is higher than the available solar maximum power (residual power $P_{res}>0$), and the residual power demand is higher than the fuel cell threshold, the fuel cell will be turned on at its own power threshold and the extra-power will be supplied by the battery. In this condition all three sources are ON. Otherwise, if the residual power demand is lower than the fuel cell power threshold, the fuel cell will supply the residual energy if the battery SOC is higher than 90% or, if the battery SOC is less than 90%, the fuel cell will be set at its own power threshold, thus providing both battery charging and load supply. In this condition PV and fuel cell are ON and the battery will source or sink the extra-power according to its own SOC.

If the instantaneous power demand is lower than the available solar maximum power ($P_{res}<0$), if the battery is fully charged (SOC>90%), the solar power will be disconnected, and the battery will entirely supply the load. Otherwise, if the battery SOC is less than 90% the PV source will be enabled, the fuel cell will be turned off and the battery will sink the extra-power.

Another power sharing algorithm, namely PM2, is implemented to reduce transients of the fuel cell equivalent load, thus minimizing degradation and aging phenomena. According to PM2, priority is given to the battery whose range of SOC relies within the range [$SOC_{min}$, $SOC_{max}$]. The fuel cell acts as a battery charger. If the battery SOC is higher than a maximum threshold $SOC_{max}$, solar power and fuel cell will be disabled. If the battery SOC lies in the range of [$SOC_{min}$, $SOC_{max}$], solar power will be enabled.

If the battery SOC is less than $SOC_{min}$, also the fuel cell will be turned on. If the solar power is higher than the load power demand and the battery SOC is higher than 90% the solar power will be disabled, thus avoiding battery overcharge conditions.

## 4. Model of the multi-source supply

The modeling approach in MATLAB/Simulink is designed to be a flexible and modular test platform that supports the addition of additional renewable sources and validates many power management algorithms. The model of the hybrid power system is implemented in MATLAB/Simulink environment. The *Mission Load*, shown in Fig. 4 serves as the model input. The model accurately computes electrical quantities and datasets, concerning PV source, the battery and the fuel cell, which may be conveniently used as system performance indicators. The proposed model also allows the designer to assess the size criteria of the whole power system, including the primary power sources. Thanks to the *Input Mission Section*, shown in Fig. 5, in the implemented model, the user easily interacts with the simulation setup by selecting the reference mission, the power management algorithm, auxiliary parts to be activated, two sliders to fix $SOC_{min}$ and $SOC_{max}$ parameters for PM2 algorithm and even a switch to whether add the PV modules or not. The

**Table 1**
Technical specifications of on-board power sources.

| *Photovoltaic modules (Solbian)* | | |
|---|---|---|
| *Parameters* | *SP72C* | *SP104C* |
| Maximum Power Pmax [W] | 72,0 | 104,0 |
| Length [mm] | 840 | 1065 |
| Width: [mm] | 556 | 585 |
| Thickness [mm] | 2,0 | 2,0 |
| Weight [kg] | 1,0 | 1,4 |
| Voltage at maximum power point Vmp [V] | 12,6 | 18,2 |
| Current at maximum operating point Imp [A] | 5,7 | 5,7 |
| Open circuit voltage Vca [V] | 15,1 | 21,8 |
| Short circuit current Icc [A] | 6,0 | 6,0 |
| Nominal Operating Cell Temperature NOCT [°C] | 45 ± 2 | 45 ± 2 |
| Operating Temperature [°C] | −40/ +85 | −40/ +85 |
| Temperature Coefficient of Pmax [%/°C] | −0,38 | −0,38 |
| Temperature coefficient of open circuit voltage Vca [%/°C] | −0,27 | −0,27 |
| Temperature coefficient of short circuit current Icc [%/°C] | 0,05 | 0,05 |
| *Horizon Fuel Cell Technologies Inc H-300 Stack* | | |
| Type | PEM | |
| Number of cells | 60 | |
| Nominal power | 300 [W] | |
| Maximum rated power | 330 [W] | |
| Performances | 36 [V] @ 8,3 [A] | |
| Operating voltage range | 30 ÷ 57,19 [V] | |
| Reactants | Air and hydrogen | |
| Stack maximum temperature | 65 °C | |
| Hydrogen pressure range | 0,45 ÷ 0,55 [bar] | |
| Weight | 2,79 [kg] | |
| Size | 11,8 × 26,2 × 9,4 [cm] | |
| Stack efficiency | 40 % @ 36 [V] | |
| Over-temperature protection threshold | 65 °C | |
| Under-voltage protection threshold | 30 [V] | |
| Over-current protection threshold | 12 [A] | |
| *MyH2-900 Hydrogen reserve bottle* | | |
| Storage capability | 900 [lt] | |
| External bottle volume | 1,7 [lt] | |
| Weight | 6,9 [kg] | |
| Dimensions | 38 × 10 cm (HxD) | |
| Hydrogen minimum purity | 99,995 % | |
| Maximum rated pressure | 30 [bar] | |
| *IS36V15 Lithium-ion Battery Pack* | | |
| Technology | Lithium-ion | |
| Rated capacity | 15 [Ah] @ 0.2C | |
| Nominal voltage | 36 [V] | |
| Maximum recharge voltage | 42 [V] | |
| Cell configuration | *Li-ion 18650*: 10S5P | |
| Weight | 2,3 [kg] | |
| Dimensions | 7,60 × 7,00 × 25,70 [cm] | |

model allows to investigate performances of the implemented algorithms, simulating the behavior of the multi-source energy system as closely as possible to its effective behavior.

Battery source is modelled by *Battery* block, which is available in Simulink libraries, by setting parameters from the datasheet of the commercial device. From the block measurement bus, battery SOC can be observed. Fuel cell source is modelled by fitting the steady state V–I curve [50], which is available in the datasheet of commercial device. By means of hydrogen flow versus power, which is supplied by datasheet of the commercial device, residual liters of hydrogen are computed within the fuel cell subsystem. Irradiance and temperature, as derived from PVGIS online tool, are set as the input of the PV modules. As shown in the PV section of Fig. 6, a switch block is driven by the switch of the input section, which can activate or disable the PV source. The PV produced power is subtracted to the input mission profile to calculate the residual power used in the *Power Management Section,* which is shown in Fig. 7. The power management unit output the power setpoint for both the fuel cell and the battery according to simulated power management algorithm. The corresponding power setpoint is forced within the *Fuel cell Section* and the *Battery section* of the model, as shown in Fig. 6.

The power consumption profiles of the reference missions are stored and imported in the MATLAB workspace. By the "*Mission Loads*" subsystem, as shown in Fig. 7, the model generates the instantaneous power consumption profile (*P_mission*) of the user-selected mission as a function of time *P(t)*. Mission profiles include all auxiliary parts active by default. Then, in case of partial activation, the counterpart consumption is subtracted to the mission profile to calculate the effective mission profile as selected by user. The PV produced power is subtracted to the updated mission profile to calculate the residual power, which is an input of the power management unit. The subsystem "*To DC bus*" outputs the DC bus current profile and the drawn power profile from the mission profile, by assuming the DC bus voltage constant at its nominal value of 48 [V].

Because of the discrepancy between the converter switching frequency and the total time of reference missions, the power converters are here modelled through elementary "*Gain*" library blocks, emulating the typical value of the corresponding power conversion efficiency, derived from datasheet of the commercial device. According to the selected power management algorithm, the "*Power Management Algorithm*" subsystem generates the equivalent power profile to be drawn from the battery section and from the fuel cell section, *P_batt* and *P_fc* respectively, accounting for the front-end converters by the gain elements.

Thanks to the proposed model structure, the instantaneous power profiles supplied by the battery and the fuel cell to meet the overall mission requirements are simulated, also accounting for power losses in the front-end converters.

## 5. Simulation results and discussion

The proposed model allows the simulation of the SWAMP reference mission to evaluate behavior and performances of the multi-source power supply system, by setting the mission, algorithm parameters, enabled/disabled PV source and auxiliary parts to be activated in the corresponding blocks of the *Input Section*. SWAMP_A mission features the highest energy consumption (1616 [Wh]) and the longest duration (355.32 min). The simulations are performed by forcing a 25 °C Battery temperature and a 300 [W] fuel cell power threshold (PFC). Simulation results and waveforms under PM2 during mission SWAMP_A are presented and discussed in this section. Fig. 8 shows the PV production in the selected day of the year (June 21, 2019) during mission SWAMP_A execution. At the bottom on the right is shown the mission power profile in violet and the net mission power in brown. As shown by the instantaneous power profile, fast load current transients occur during the mission execution. The net mission power is obtained as the mission power minus the PV generated power. The profile of PV generated power is obtained by PVGIS online tool for the selected day and starting hour of the executed mission.

In Fig. 8, the net power generated by the two PV modules, PV104 and PV72 respectively, are shown. The total power PV Power is obtained as the sum of PV104 and PV72 due to modules connections. The produced power is close to the maximum theoretical value, approximately in the middle of the mission period of execution. The PV power is a consequence of the irradiance and temperature of the selected location, date and starting time. The load net power, shown in brown in Fig. 8 equals the power that will be supplied by the fuel cell and the battery, according to the selected power management algorithm.

The system is simulated under PM2 selecting 50% as the $SOC_{min}$ parameter. As shown in Fig. 9, when the battery SOC approaches the $SOC_{min}$ value, the system will start to recharge the battery by means of extra-power available on board and eventually turning on the fuel cell. During recharge, the battery sinks the current, which is negative and equal to the extra-power. When the battery SOC approaches the $SOC_{max}$

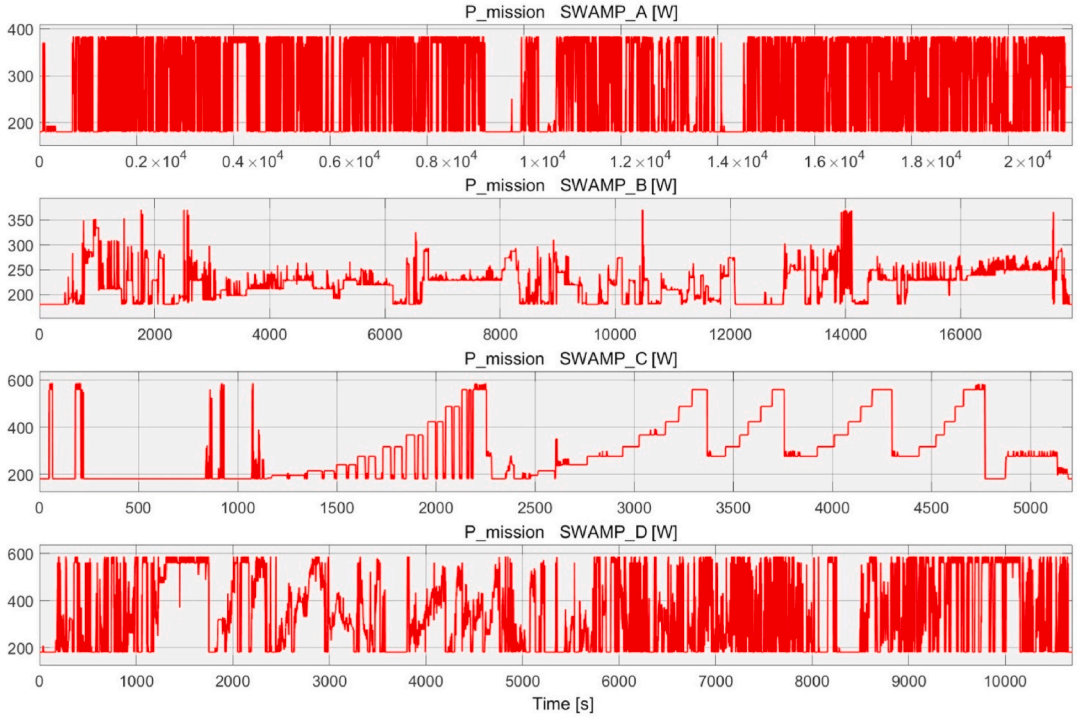


**Fig. 3.** -Recorded experimental power consumption profiles of the battery-operated SWAMP prototype during four reference water missions. SWAMP_A mission has been recorded in Camogli (Italy), SWAMP_B and SWAMP_C in Biograd Na Moru (Croatia) and SWAMP_D mission in Roja (Italy).

**Table 2**
Parameters of four relevant experimental water mission of the battery-operated SWAMP vehicle.

| Parameter | Reference Mission | | | |
|---|---|---|---|---|
| Reference name (SWAMP_*) | A | B | C | D |
| Duration [min] | 355.32 | 299.01 | 86.85 | 178.24 |
| Average power [W] | 272.90 | 221.16 | 295.46 | 329.31 |
| Peak power [W] | 383.20 | 370.20 | 586.20 | 586.20 |
| Required energy [Wh] | 1616.14 | 1102.14 | 427.70 | 978.23 |

parameter value, discharge begins, and the fuel cell will be turned off. Battery voltage follows the discharge and charge characteristics of the selected battery. The Depth of Discharge of the battery is limited to 40% thus preserving battery life.

As shown in Fig. 10, the fuel cell is turned on to recharge the battery with a constant current, thus acting as a range extender when required. The fuel cell equivalent load remains constant regardless of the mission power profile, thereby safeguarding the fuel cell from degradation and aging.

By comparing Figs. 9 and 10, the fuel cell turns on when the battery SOC approaches the minimum allowable value of $SOC_{min}$ to recharge the battery. The battery current and the battery power, as shown in Fig. 9,

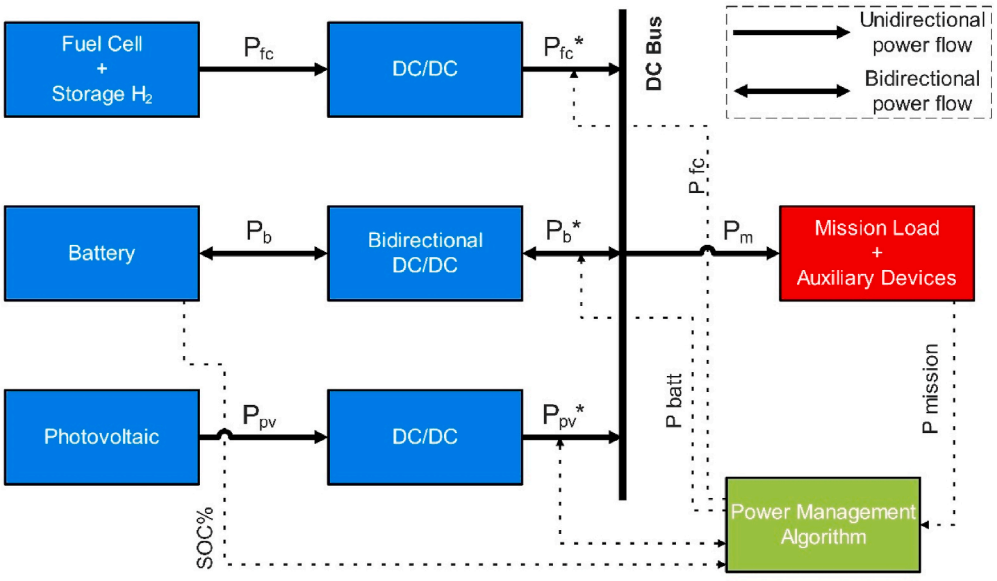


**Fig. 4.** Multi-source energy system.

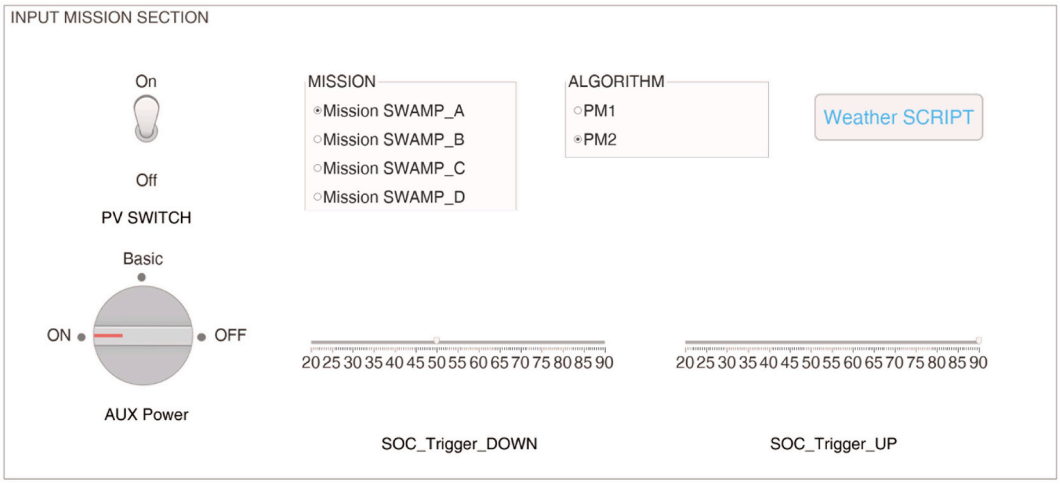


**Fig. 5.** Model of the dashboard for input section.

are negative validating the charge phase of the battery. All the sources are turned on under these operating conditions. When the battery is charged up to the maximum state of charge $SOC_{max}$, the fuel cell is turned off and the load is entirely supplied by the battery and the PV modules. The same circumstances happen at about 18000 s. Note that during battery charge phase, the net load power is lower than the fuel cell power threshold of 300 W, as shown in Fig. 8. As shown by simulation results, under PM2 algorithm the fuel cell works as a range extender, charging the battery when required.

## 6. Comparison of multi-source configurations

In Table 3, simulation results in hybrid fuel cell – battery configuration are presented. By means of the hydrogen flow versus power datasheet curve, the residual number of liters is calculated by system simulation. The percentage of residual SOC is calculated by the battery model at the end of system simulation. As shown by simulation results, the algorithm PM2 preserves the hydrogen reserve at the expense of battery charge. On the contrary, the algorithm PM1 preserves the battery charge at the expense of hydrogen reserve. Even in a dual source configuration, the system can complete the water missions, independently of the day of the year. Note that results without the solar source do not depend on the day of the year because hydrogen reserve and battery are used as the sources, which in turn are independent of the day of the year. SWAMP_A, which features the highest energy demand and the highest execution time, is completed with depleted hydrogen reserve with PM1 and a minimum amount of hydrogen reserve with PM2. SWAMP_A can be assumed as the worst case among the other missions. During mission SWAMP_A the hydrogen reserve is depleted and a SOC of 71,05% with PM1 and 62,33% with PM2 is left after the mission is completed. Note that SWAMP_A requires the highest energy among four reference missions. Notwithstanding this, the SWAMP can complete the mission even in a basic fuel cell-battery configuration. The results confirm that PM1 saves the battery charge at the expense of hydrogen reserve. In fact, the same mission with PM2 ends with 7.18 L of hydrogen and lower battery charge (62.33% instead of 71.05%). The same trend can be observed though all the simulation results: under PM1 the remaining hydrogen is less than PM2, whereas the battery charge with PM1 is higher than that of PM2.

In Table 4, a comparison between simulation results is shown, calculating the percentage of mission energy demand covered by PV energy, as of June 21, 2019, during four reference missions and under both power management algorithms. The percentage of energy demand supplied by generated PV energy spans from 34% to 56% with enabled auxiliary parts and from 42 to even 79% enabling necessary auxiliary parts only. Note that simulation refers to the most favorable day among the selected four, that is June 21, 2019. The result with PV OFF reduces to the hybrid configuration of fuel cell – battery, reported in Table 3, being the same independently of the day of the year of mission execution. By comparing results with PV ON and PV OFF, reported in Tables 4 and 3, respectively, savings of hydrogen reserve lies in the range from 19.25 to 468.34 L. Furthermore, saving of state of charge ranges from −9.15% to 50.33%. The negative value should be interpreted as a partial gain in battery SOC without PV modules even if the hydrogen reserve diminishes to cover the lack of the PV modules. By comparing simulation results being the same the reference mission, the PM2 algorithm save higher amount of hydrogen reserve stressing more the battery source whereas PM1 preserve the battery using a higher amount of hydrogen, as shown in Table 4. The behavior is due to sources priorities established by the specific power management algorithm, as validated by simulation results. As shown by simulation results, with aux at half power (only necessary auxiliary parts active), the amount of consumed energy is different being the same the water mission. This happens because the solar power is higher than the auxiliary parts power demand and, in some intervals, the solar source is disabled, according to the peculiarities of power management algorithm. Note that the SWAMP can execute different missions consecutively, without returning to the land docking station. Energy reserve on board after the mission execution is a key parameter to account for.

Simulation results on December 21, 2019 are reported in Table 5. The percentage of energy demand covered by solar source spans from 1% to 13% with enabled auxiliary parts and from 2 to even 18% enabling necessary auxiliary parts only. Note that simulation refers to the least favorable day among the selected four, that is December 21, 2019. By comparing results with PV ON and results with PV OFF, reported in Tables 5 and 3, respectively, savings on hydrogen reserve lies in the range from 3 to 204.12 L. Furthermore, saving of state of charge ranges from −9.91% to 25.3%. The negative value should be interpreted as a partial gain in battery SOC without PV modules even if, in this case, the hydrogen reserve diminishes to cover the lack of the PV modules.

As shown in Table 5, the contribution of solar power is relevant to the energy demand only in specific days of the year. The modular architecture allows to remove the PV source on-board of the SWAMP without the need for modifying the power sharing algorithm, which self-adapts for the lack of PV solar source.

Mission SWAMP_A has been repeated two consecutive times, to calculate the gain of the vehicle endurance. Simulation results are reported in Table 6. *Date, mode and algorithm* are reported, referred to SWAMP_A mission. The *Time left* column reports the remaining time following the depletion of on-board energy reserve, given in minutes. Δ

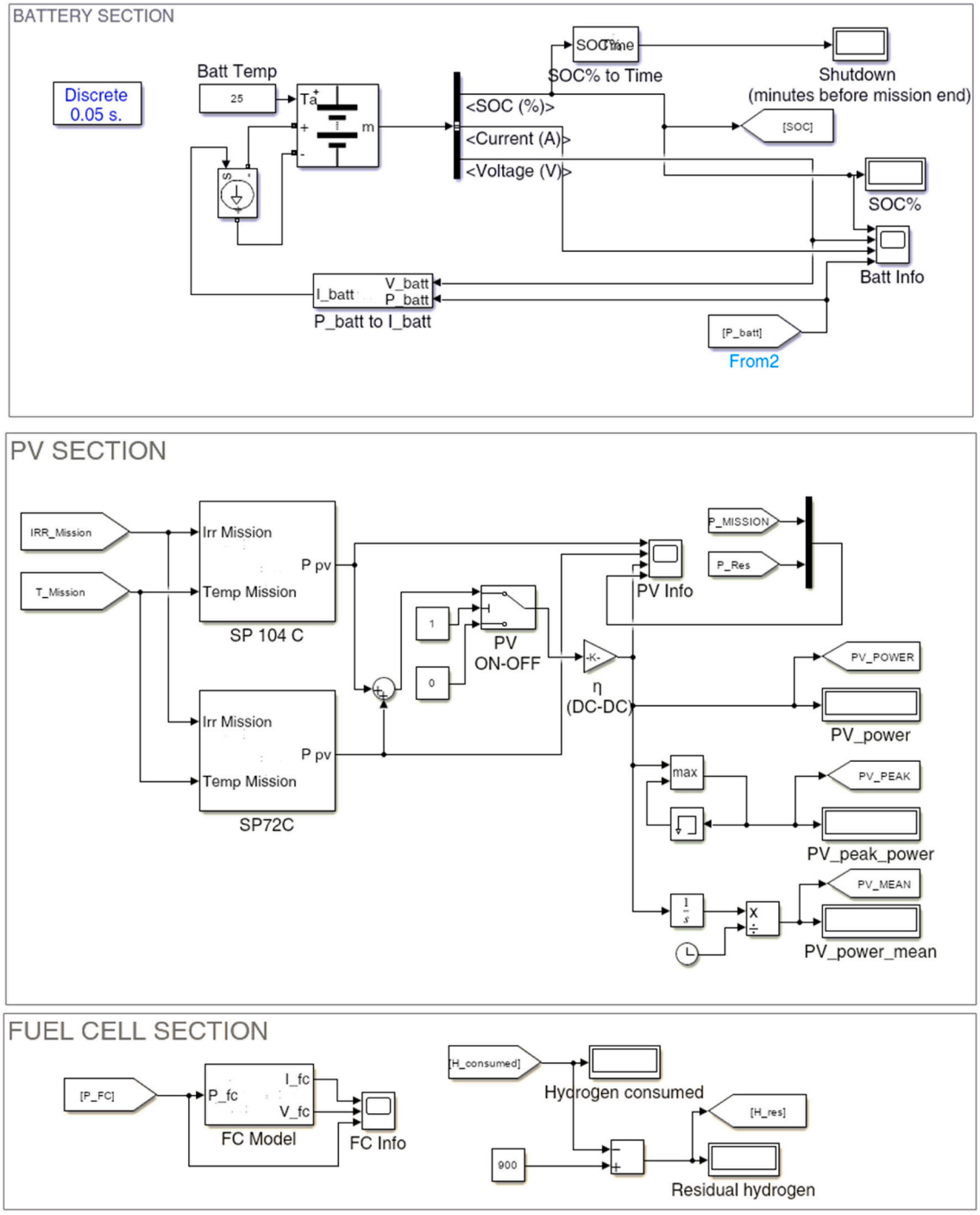


**Fig. 6.** Model of sources in MATLAB/Simulink environment. From the top to the bottom, the Battery section, the PV section and the fuel cell section.

*Endurance* column reports the relative increase of endurance in hours compared to mission SWAMP_A execution time.

In the case of partially activated auxiliaries, the second mission is also completed with no time left and therefore the endurance extension is about 6 h, that is the SWAMP_A period of execution. With auxiliary on, the second SWAMP_A mission is not entirely completed and on-board energy reserve is depleted before the end of the second mission. In these cases, the gain of endurance spans in the range from 2h25m50s (on December 21, 2019) to 5h46m05s (on June 21, 2019). With auxiliary partially activated, the doubled simulated mission is completed and a 5h55 m gain of endurance is achieved. Simulation results validate June as the most favorable day among four selected dates. Therefore, the PV modules connection may extend the vehicle single fill up cruising range up to about 11–12 h in the most favorable environmental conditions. The gain value is double the endurance with the hybrid fuel cell – battery configuration.

The battery-operated SWAMP is equipped with four batteries, each one housed in a waterproof canister for a total weight of 13.6 kg, running two at once. To achieve an endurance of 6 h, as in SWAMP_A mission, hot swap of batteries is required, with a depth of discharge of 80%. The hybrid fuel cell – battery configuration is defined with a single battery and a fuel cell on the top of the SWAMP, with a total weight of 12.39 kg and 14.79 kg if PV modules are added. Therefore, if compared with fuel cell – battery hybrid configuration, adding 2.4 kg of PV

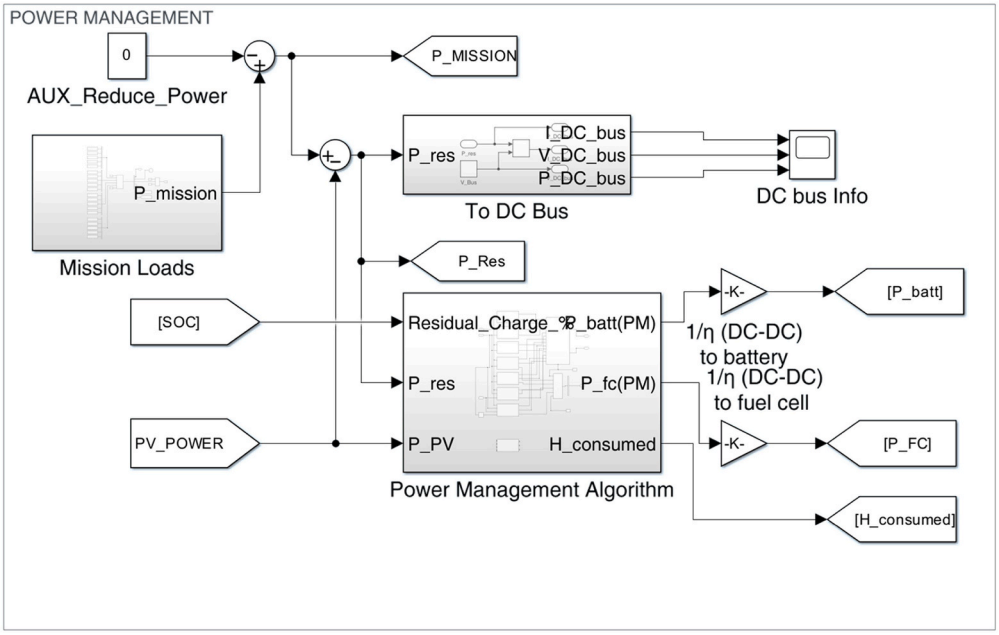


**Fig. 7.** Model of the power management unit.

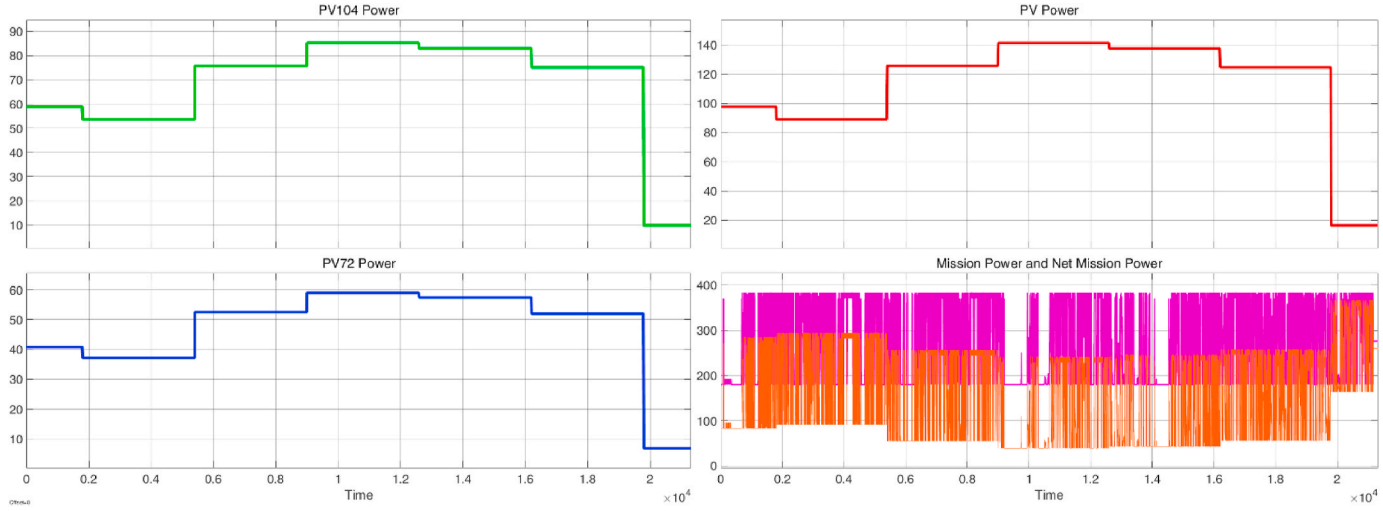


**Fig. 8.** PV production during mission SWAMP_A and consumption by SWAMP vehicle under PM2 algorithm.

modules results in an almost doubled endurance in the most favorable dates. The system is modular. This means that, on less favorable dates, the photovoltaic modules can be easily removed while still achieving 6 h of autonomy. A weight of 27.2 kg would be obtained to gain 12 h of endurance with a sole battery configuration, thus covering all the available payload for on-board instrumentation. A comparison in terms of weight is reported in Table 7.

## 7. Conclusions

In this paper, a comparison between different multi-source configurations on-board of the vehicle SWAMP has been carried out. Experimental dataset of the battery counterpart has been considered as input reference of the multi-source model. A PV – Fuel cell – Battery source has been compared with the hybrid fuel cell – battery counterpart, being the same the vehicle SWAMP. The focus of the paper is a reasonable comparison of multi-source configurations on the same vehicle under study, that is the same the weight, size and cost constraints. In a bottom-up design flow, the novelty comes from the challenges dictated by the specific applications, extends to implemented solutions and obtained results, which can be compared to recent literature data reported in Section 2. Really, the comparison with the literature data would be outperformed if the weight of the vehicle under test and related constraints in terms of size, weight and cost are considered. The specific application on small size ASV poses new challenges and strict constraints on weight and dimensions of the whole power supply system. Results are also due to the optimal power management algorithms that properly account for this limitation. Rule-based algorithms are implemented, featuring extremely low complexity of implementation. The low complexity does not affect the result.

After introducing PV modules, a feasibility analysis is conducted from both physical and mechanical perspectives, ensuring the validation of the multi-source architecture aboard the SWAMP. Power management algorithms are designed self-accommodating in case of disabled PV modules. The MATLAB/Simulink modeling approach is conceived as a modular and flexible testing platform to validate various power

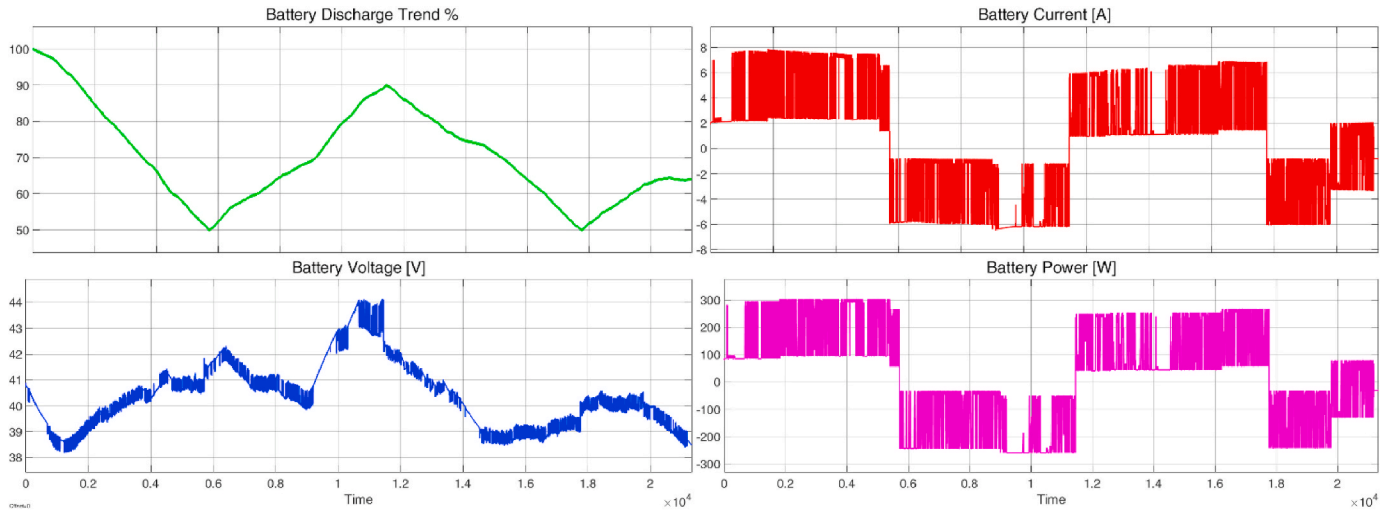


**Fig. 9.** Battery waveforms during mission SWAMP_A under PM2 algorithm.

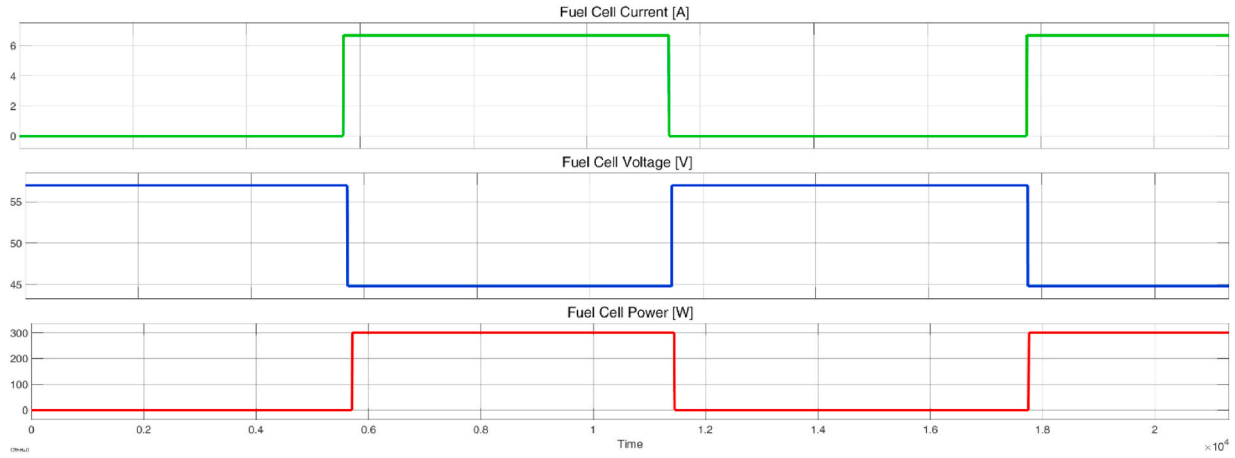


**Fig. 10.** Fuel cell waveforms during mission SWAMP_A under PM2 algorithm.

**Table 3**
Simulation results in a fuel cell - battery hybrid configuration.

| Mode | Mission | Algorithm | SOC res [%] | H2 res [l] |
|---|---|---|---|---|
| AUX ON PV OFF | SWAMP_A | PM1 | 71.05% | 0.00 |
| | | PM2 | 62.33% | 7.18 |
| | SWAMP_B | PM1 | 75.84% | 746.50 |
| | | PM2 | 41.34% | 855.47 |
| | SWAMP_C | PM1 | 84.01% | 366.72 |
| | | PM2 | 41.27% | 492.58 |
| | SWAMP_D | PM1 | 36.59% | 570.79 |
| | | PM2 | 8.68% | 656.78 |
| AUX HALF PV OFF | SWAMP_A | PM1 | 91.94% | 195.22 |
| | | PM2 | 58.47% | 261.93 |
| | SWAMP_B | PM1 | 85.58% | 766.81 |
| | | PM2 | 48.66% | 879.48 |
| | SWAMP_C | PM1 | 99.15% | 501.52 |
| | | PM2 | 79.00% | 549.71 |
| | SWAMP_D | PM1 | 68.05% | 577.94 |
| | | PM2 | 35.49% | 679.37 |

management algorithms and facilitate the integration of other renewable sources. A comparison between different multi-source configurations on-board of the vehicle SWAMP has been carried out. An endurance up to 6 or 12 h is achieved with disabled or enabled PV, respectively. The absolute extended cruising range varies based on the specific day and start time due to fluctuating climate conditions. Yet, the modular architecture allows removing the PV source on-board of the SWAMP without the need for modifying the power sharing algorithm, which self-accommodates for the lack of PV solar source.

The presented sizing and optimization method can be adapted for the use in other sites and marine vehicles. The most challenging scenario for sizing and optimization is represented by the extremely lightweight SWAMP vehicle. However, the model can be easily expanded to include additional locations by accessing irradiance and temperature data from the PVGIS online tool and easily importing them into the model. Moreover, this model can be extended to accommodate other marine vehicles by incorporating their instantaneous power profiles into the mission profile section or by integrating a model of the new marine vehicle directly into MATLAB/Simulink.

## CRediT authorship contribution statement

**A. Riccobono:** Writing – review & editing, Resources, Methodology, Investigation, Formal analysis, Data curation, Conceptualization. **V. Boscaino:** Writing – review & editing, Writing – original draft, Validation, Supervision, Resources, Methodology, Investigation, Formal analysis, Data curation, Conceptualization. **A. Odetti:** Writing – review & editing, Writing – original draft, Resources, Project administration, Funding acquisition, Data curation, Conceptualization. **F.P. Mammana:** Methodology, Investigation, Formal analysis, Conceptualization. **G. Cipriani:** Writing – review & editing, Writing – original draft,

**Table 4**
Comparison of simulation results on June 21, 2019.

| Operating mode | Mission | Algorithm | SOC res [%] | H2 res [l] | $E_{PV}$ consumed [Wh] | % energy demand |
|---|---|---|---|---|---|---|
| AUX ON | SWAMP_A | PM1 | 99.97% | 406.28 | 679.65 | 42% |
| PV ON | | PM2 | 71.41% | 417.14 | 679.65 | 42% |
| | SWAMP_B | PM1 | 90.24% | 797.4 | 163.47 | 38% |
| | | PM2 | 55.75% | 898.73 | 163.47 | 38% |
| | SWAMP_C | PM1 | 99.91% | 672.42 | 622.40 | 56% |
| | | PM2 | 87.98% | 683.59 | 622.40 | 56% |
| | SWAMP_D | PM1 | 86.92% | 608.09 | 328.66 | 34% |
| | | PM2 | 56.23% | 703.2 | 328.66 | 34% |
| AUX HALF | SWAMP_A | PM1 | 90.00% | 610.71 | 585.04 | 47% |
| PV ON | | PM2 | 55.62% | 705.51 | 693.14 | 56% |
| | SWAMP_B | PM1 | 92.00% | 832.42 | 152.62 | 45% |
| | | PM2 | 69.44% | 898.73 | 157.07 | 47% |
| | SWAMP_C | PM1 | 90.00% | 821.81 | 552.70 | 70% |
| | | PM2 | 70.34% | 895.62 | 620.77 | 79% |
| | SWAMP_D | PM1 | 86.26% | 709.30 | 334.29 | 42% |
| | | PM2 | 62.42% | 778.92 | 335.90 | 43% |

**Table 5**
Comparison of simulation results on December 21, 2019.

| Operating mode | Mission | Algorithm | SOC res [%] | H2 res [l] | $E_{PV}$ consumed [Wh] | % energy demand |
|---|---|---|---|---|---|---|
| AUX ON | SWAMP_A | PM1 | 90.00% | 122.39 | 207.03 | 13% |
| PV ON | | PM2 | 52.42% | 211.3 | 207.03 | 13% |
| | SWAMP_B | PM1 | 78.15% | 750.06 | 3.64 | 1% |
| | | PM2 | 42.79% | 860.81 | 3.64 | 1% |
| | SWAMP_C | PM1 | 91.34% | 393.35 | 44.53 | 4% |
| | | PM2 | 54.00% | 502.04 | 44.53 | 4% |
| | SWAMP_D | PM1 | 61.89% | 573.8 | 114.03 | 12% |
| | | PM2 | 32.27% | 666.75 | 114.03 | 12% |
| AUX HALF | SWAMP_A | PM1 | 99.98% | 355.38 | 221.45 | 18% |
| PV ON | | PM2 | 64.24% | 394.30 | 221.45 | 18% |
| | SWAMP_B | PM1 | 87.39% | 771.84 | 7.16 | 2% |
| | | PM2 | 50.45% | 883.75 | 7.16 | 2% |
| | SWAMP_C | PM1 | 99.60% | 545.53 | 56.67 | 7% |
| | | PM2 | 87.26% | 566.41 | 56.67 | 7% |
| | SWAMP_D | PM1 | 85.62% | 602.21 | 121.26 | 15% |
| | | PM2 | 53.83% | 701.11 | 121.26 | 15% |

**Table 6**
Simulation results under two consecutive SWAMP_A mission executions.

| Date | Mode | Algorithm | Time left [h:mm:ss] | Δ Endurance [h:mm:ss] |
|---|---|---|---|---|
| 21/3/2019 | AUX ON | PM1 | 0:41:43 | 5:13:36 |
| | | PM2 | 1:28:04 | 4:27:16 |
| | AUX HALF | PM1 | 0 | 5:55:19 |
| | | PM2 | 0 | 5:55:19 |
| 21/6/2019 | AUX ON | PM1 | 0:09:14 | 5:46:05 |
| | | PM2 | 0:58:13 | 4:57:06 |
| | AUX HALF | PM1 | 0 | 5:55:19 |
| | | PM2 | 0 | 5:55:19 |
| 21/9/2019 | AUX ON | PM1 | 1:40:58 | 4:14:22 |
| | | PM2 | 2:18:43 | 3:36:36 |
| | AUX HALF | PM1 | 0 | 5:55:19 |
| | | PM2 | 0 | 5:55:19 |
| 21/12/2019 | AUX ON | PM1 | 3:03:02 | 2:52:17 |
| | | PM2 | 3:29:29 | 2:25:50 |
| | AUX HALF | PM1 | 0 | 5:55:19 |
| | | PM2 | 0:52:52 | 5:02:28 |

**Table 7**
Weight and endurance comparison of configurations under study.

| Configuration | Weight | Endurance |
|---|---|---|
| Battery original configuration | 13.6 kg | Up to 6 h |
| FC-Battery | 12.39 kg | Up to 6 h |
| PV- FC – Battery | 14.79 kg | Up to 12 h |
| Battery configuration 2 | 27.2 kg | Up to 12 h |

Supervision, Resources, Methodology, Investigation, Formal analysis, Data curation, Conceptualization. **G. Bruzzone:** Writing – review & editing, Supervision, Resources, Data curation. **V. Di Dio:** Writing – review & editing, Validation, Supervision, Conceptualization. **M. Caccia:** Writing – review & editing, Supervision, Resources, Data curation. **G. Tinè:** Writing – review & editing, Validation, Supervision, Data curation, Conceptualization.

## Declaration of competing interest

The authors declare that they have no known competing financial interests or personal relationships that could have appeared to influence the work reported in this paper.

## Acknowledgements

Authors wish to thank the technical staff composed by Simona Aracri, Marco Bibuli, Giorgio Bruzzone, Mauro Giacopelli, Roberta Ferretti, Edoardo Spirandelli and Enrica Zereik for their contribution in the design, construction and testing of the mechanical and electrical systems of the robotic platform.

The research is supported by the project “Robotics and AI for Socio-economic Empowerment” (Project acronym: RAISE), within the framework of the Italian National Recovery and Resilience Plan (NRRP), Mission 4, Component 2, Investment 1.5, CUP B33C22000700006.

## References


[1] Mokhtara C, Negrou B, Settou N, Settou B, Samy MM. Design optimization of off-grid Hybrid Renewable Energy Systems considering the effects of building energy performance and climate change: case study of Algeria. Energy 2021;219:119605. https://doi.org/10.1016/j.energy.2020.119605.

[2] Barakat S, Osman AI, Tag-Eldin E, Telba AA, Abdel Mageed HM, Samy MM. Achieving green mobility: multi-objective optimization for sustainable electric vehicle charging. Energy Strategy Rev 2024;53(February):101351. https://doi.org/10.1016/j.esr.2024.101351.

[3] IMO. Fourth IMO GHG study 2020 full report. 2021.

[4] International Maritime Organization. IMO Strategy on reduction of GHG emissions from ships. 2023. 2023.

[5] Xu H, Moreira L, Guedes Soares C. Maritime autonomous vessels. J Mar Sci Eng 2023;11(1):10–2. https://doi.org/10.3390/jmse11010168.

[6] Zhang Y, Shi G, Liu J. Dynamic energy-efficient path planning of unmanned surface vehicle under time-varying current and wind. J Mar Sci Eng 2022;10(6). https://doi.org/10.3390/jmse10060759.

[7] Bhagavathi R, Kwame Minde Kufoalor D, Hasan A. Digital twin-driven fault diagnosis for autonomous surface vehicles. IEEE Access 2023;11(May):41096–104. https://doi.org/10.1109/ACCESS.2023.3268711.

[8] Liu Z, Zhang Y, Yu X, Yuan C. Unmanned surface vehicles: an overview of developments and challenges. Annu Rev Control 2016;41:71–93. https://doi.org/10.1016/j.arcontrol.2016.04.018.

[9] Odetti A, Bruzzone G, Altosole M, Viviani M, Caccia M. SWAMP, an Autonomous Surface Vehicle expressly designed for extremely shallow waters. Ocean Eng 2020;216:108205. https://doi.org/10.1016/j.oceaneng.2020.108205.

[10] Haxhiu A, Abdelhakim A, Kanerva S, Bogen J. Electric power integration schemes of the hybrid fuel cells and batteries-fed marine vessels - an overview. IEEE Transact Transport Electrificat 2022;8(2):1885–905. https://doi.org/10.1109/TTE.2021.3126100.

[11] Shakeri N, Zadeh M, Bremnes Nielsen J. Hydrogen fuel cells for ship electric propulsion: moving toward greener ships. IEEE Electrific Magaz 2020;8(2):27–43. https://doi.org/10.1109/MELE.2020.2985484.

[12] Cavo M, Gadducci E, Rattazzi D, Rivarolo M, Magistri L. Dynamic analysis of PEM fuel cells and metal hydrides on a zero-emission ship: a model-based approach. Int J Hydrogen Energy 2021;46(64):32630–44. https://doi.org/10.1016/j.ijhydene.2021.07.104.

[13] Dall'Armi C, Micheli D, Taccani R. Comparison of different plant layouts and fuel storage solutions for fuel cells utilization on a small ferry. Int J Hydrogen Energy 2021;46(26):13878–97. https://doi.org/10.1016/j.ijhydene.2021.02.138.

[14] Chiche A, Andruetto C, Lagergren C, Lindbergh G, Stenius I, Peretti L. Feasibility and impact of a Swedish fuel cell-powered rescue boat. Ocean Eng 2021;234(March):109259. https://doi.org/10.1016/j.oceaneng.2021.109259.

[15] Al Amerl A, Oukkacha I, Camara MB, Dakyo B. Real-time control strategy of fuel cell and battery system for electric hybrid boat application. Sustainability 2021;13(16). https://doi.org/10.3390/su13168693.

[16] Rivarolo M, Rattazzi D, Magistri L, Massardo AF. Multi-criteria comparison of power generation and fuel storage solutions for maritime application. Energy Convers Manag 2021;244(January 2020):114506. https://doi.org/10.1016/j.enconman.2021.114506.

[17] Zhang X, Liu L, Dai Y, Lu T. Experimental investigation on the online fuzzy energy management of hybrid fuel cell/battery power system for UAVs. Int J Hydrogen Energy 2018;43(21):10094–103. https://doi.org/10.1016/j.ijhydene.2018.04.075.

[18] Balestra L, Schjølberg I. Modelling and simulation of a zero-emission hybrid power plant for a domestic ferry. Int J Hydrogen Energy 2021;46(18):10924–38. https://doi.org/10.1016/j.ijhydene.2020.12.187.

[19] Renau J, Tejada D, García V, López E, Domenech L, Lozano A, Barreras F. Design, development, integration and evaluation of hybrid fuel cell power systems for an unmanned water surface vehicle. Int J Hydrogen Energy 2024;54:1273–85. https://doi.org/10.1016/j.ijhydene.2023.12.043. June 2023.

[20] Wu J, Cai S, Guan Y, Li S, Tu Z. Design and performance evaluation of power system for unmanned ship based on proton exchange membrane fuel cell. Int J Hydrogen Energy 2024;59:730–41. https://doi.org/10.1016/j.ijhydene.2024.02.063. December 2023.

[21] Chen H, Zhao X, Zhang T, Pei P. The reactant starvation of the proton exchange membrane fuel cells for vehicular applications: a review. Energy Convers Manag 2019;182:282–98. https://doi.org/10.1016/j.enconman.2018.12.049. September 2018.

[22] Bai X, Jian Q, Huang B, Luo L, Chen Y. Hydrogen starvation mitigation strategies during the start-up of proton exchange membrane fuel cell stack. J Power Sources 2022;520:230809. https://doi.org/10.1016/j.jpowsour.2021.230809. November 2021.

[23] Bernard J, Hofer M, Hannesen U, Toth A, Tsukada A, Büchi FN, Dietrich P. Fuel cell/battery passive hybrid power source for electric powertrains. J Power Sources 2011;196(14):5867–72. https://doi.org/10.1016/j.jpowsour.2011.03.015.

[24] Cheng XF, Zhao Q, Wang D, Liu C, Zhang Y. A high step-up multiphase interleaved boost converter for fuel cells power system. Int J Hydrogen Energy 2024;56:667–75. https://doi.org/10.1016/j.ijhydene.2023.12.210. December 2023.

[25] Roda V, Carroquino J, Valiño L, Lozano A, Barreras F. Remodeling of a commercial plug-in battery electric vehicle to a hybrid configuration with a PEM fuel cell. Int J Hydrogen Energy 2018;43(35):16959–70. https://doi.org/10.1016/j.ijhydene.2017.12.171.

[26] Oladosu TL, Pasupuleti J, Kiong TS, Koh SPJ, Yusaf T. Energy management strategies, control systems, and artificial intelligence-based algorithms development for hydrogen fuel cell-powered vehicles: a review. Int J Hydrogen Energy 2024;61(March):1380–404. https://doi.org/10.1016/j.ijhydene.2024.02.284.

[27] Güven AF, Yörükeren N, Samy MM. Design optimization of a stand-alone green energy system of university campus based on Jaya-Harmony Search and Ant Colony Optimization algorithms approaches. Energy 2022;253. https://doi.org/10.1016/j.energy.2022.124089.

[28] Güven AF, Mahmoud Samy M. Performance analysis of autonomous green energy system based on multi and hybrid metaheuristic optimization approaches. Energy Convers Manag 2022;269(August):116058. https://doi.org/10.1016/j.enconman.2022.116058.

[29] Ettihir K, Boulon L, Agbossou K. Optimization-based energy management strategy for a fuel cell/battery hybrid power system. Appl Energy 2016;163:142–53. https://doi.org/10.1016/j.apenergy.2015.10.176.

[30] Feroldi D, Serra M, Riera J. Energy management strategies based on efficiency map for fuel cell hybrid vehicles. J Power Sources 2009;190(2):387–401. https://doi.org/10.1016/j.jpowsour.2009.01.040.

[31] Sürer MG, Arat HT. Advancements and current technologies on hydrogen fuel cell applications for marine vehicles. Int J Hydrogen Energy 2022;47(45):19865–75. https://doi.org/10.1016/j.ijhydene.2021.12.251.

[32] Liu J, Yang F, Wu Z, Zhang Z. A review of thermal coupling system of fuel cell-metal hydride tank: classification, control strategies, and prospect in distributed energy system. Int J Hydrogen Energy 2024;51:274–89. https://doi.org/10.1016/j.ijhydene.2023.04.232.

[33] Stanghellini G, Del Bianco F, Gasperini L. OpenSWAP, an open architecture, low cost class of autonomous surface vehicles for geophysical surveys in the shallow water environment. Rem Sens 2020;12(16). https://doi.org/10.3390/rs12162575.

[34] Carlson DF, Fürsterling A, Vesterled L, Skovby M, Pedersen SS, Melvad C, Rysgaard S. An affordable and portable autonomous surface vehicle with obstacle avoidance for coastal ocean monitoring. HardwareX 2019;5:1–20. https://doi.org/10.1016/j.ohx.2019.e00059.

[35] Ferri G, Manzi A, Fornai F, Ciuchi F, Laschi C. The HydroNet ASV, a small-sized autonomous catamaran for real-time monitoring of water quality: from design to missions at sea. IEEE J Ocean Eng 2015;40(3):710–26. https://doi.org/10.1109/JOE.2014.2359361.

[36] Duranti P. CatOne, multitask unmanned surface vessel for hydro-geological and environment surveys. In: Lollino G, Arattano M, Rinaldi M, Giustolisi O, Marechal J-C, Grant GE, editors. Engineering geology for society and territory - volume 3. Cham: Springer International Publishing; 2015. p. 647–52.

[37] Boscaino V, Odetti A, Marsala G, Di Cara D, Panzavecchia N, Caccia M, Tinè G. A fuel cell powered autonomous surface vehicle: the Eco-SWAMP project. Int J Hydrogen Energy 2021;46(39):20732–49. https://doi.org/10.1016/j.ijhydene.2021.03.158.

[38] Elkafas AG, Rivarolo M, Gadducci E, Magistri L, Massardo AF. Fuel cell systems for maritime: a review of research development, commercial products, applications, and perspectives. Processes 2023;11(1). https://doi.org/10.3390/pr11010097.

[39] Sohn SI, Oh JH, Lee YS, Park DH, Oh IK. Design of a fuel-cell-powered catamaran-type unmanned surface vehicle. IEEE J Ocean Eng 2015;40(2):388–96. https://doi.org/10.1109/JOE.2014.2315889.

[40] Han J, Charpentier JF, Tang T. An energy management system of a fuel cell/battery hybrid boat. Energies 2014;7(5):2799–820. https://doi.org/10.3390/en7052799.

[41] Dall'Armi C, Pivetta D, Taccani R. Hybrid PEM fuel cell power plants fuelled by hydrogen for improving sustainability in shipping: state of the art and review on active projects. Energies 2023;16(4). https://doi.org/10.3390/en16042022.

[42] Boukoberine MN, Zhou Z, Benbouzid M, Donateo T. A frequency separation rule-based power management strategy for a hybrid fuel cell-powered drone. In: IECON proceedings (industrial electronics conference); 2020. p. 4975–80. https://doi.org/10.1109/IECON43393.2020.9255118.

[43] Boukoberine MN, Zia MF, Benbouzid M, Zhou Z, Donateo T. Hybrid fuel cell powered drones energy management strategy improvement and hydrogen saving using real flight test data. Energy Convers Manag 2021;236(December 2020):113987. https://doi.org/10.1016/j.enconman.2021.113987.

[44] Boukoberine MN, Donateo T, Benbouzid M. Optimized energy management strategy for hybrid fuel cell powered drones in persistent missions using real flight test data. IEEE Trans Energy Convers 2022;37(3):2080–91. https://doi.org/10.1109/TEC.2022.3152351.

[45] Zixuan Wang KJ, Liu Zhi, Fan Linhao, Du Qing. Application progress of small-scale proton exchange membrane fuel cell. Energy Rev 2023:1–40. https://doi.org/10.1016/j.enrev.2023.100017.

[46] Rafiei M, Boudjadar J, Khooban MH. Energy management of a zero-emission ferry boat with a fuel-cell-based hybrid energy system: feasibility assessment. IEEE Trans Ind Electron 2021;68(2):1739–48. https://doi.org/10.1109/TIE.2020.2992005.

[47] De Lorenzo G, Piraino F, Longo F, Tin G, Boscaino V, Panzavecchia N, Caccia M, Fragiacomo P. Modelling and performance analysis of an autonomous marine vehicle powered by a fuel cell hybrid powertrain. Energies 2022;15(19):1–21.

[48] Odetti A M, Altosole M, Bibuli M, Bruzzone G, Caccia, Viviani M. Advance speed-hull-pump-jet interactions in small ASV. In: Volume 5: HSMV 2020, series progress in marine science and technology. IOS Press; 2020. p. 197–206. https://doi.org/10.3233/PMST200043.

[49] Pellegrini R, Ficini S, Odetti A, Serani A, Caccia M, Diez M. Multi-fidelity hydrodynamic analysis of an autonomous surface vehicle at surveying speed in deep water subject to variable payload. Ocean Eng 2023;271(September 2022):113529. https://doi.org/10.1016/j.oceaneng.2022.113529.

[50] Boscaino V, Miceli R, Capponi G. MATLAB-based simulator of a 5 kW fuel cell for power electronics design. Int J Hydrogen Energy 2013;38(19):7924–34. https://doi.org/10.1016/j.ijhydene.2013.04.123.